CCFE
CULHAM CENTRE FOR FUSION ENERGY

CCFE-PR(16)82

S.C. Chapman, R.O. Dendy, P.T. Lang, N.W. Watkins,
F.A. Calderon, M. Romanelli, T.N. Todd and JET
Contributors

The global build-up to intrinsic ELM bursts and comparison with pellet precipitated ELMs seen in JET

The global build-up to intrinsic ELM bursts and comparison with pellet precipitated ELMs seen in JET

S.C. Chapman[1], R.O. Dendy[2,1], P.T. Lang[3], N.W. Watkins[1,4,5],
F.A. Calderon[1], M. Romanelli[2], T.N. Todd[2] and JET Contributors

[1] Centre for Fusion, Space and Astrophysics, Department of Physics, University of Warwick, Coventry, UK
[2] CCFE, Culham Science Centre, Abingdon, Oxfordshire OX14 3DB, UK
[3] Max-Planck-Institut für Plasmaphysik, Garching, Germany
[4] Centre for the Analysis of Time Series, London School of Economics, London, UK
[5] Dept. of Engineering and Innovation, Open University, Milton Keynes, UK

The global build-up to intrinsic ELM bursts and comparison with pellet precipitated ELMs seen in JET

S. C. Chapman[1],* R. O. Dendy[2,1], P. Lang[3], N. W. Watkins[1,4,5],
F. A. Calderon[1], M. Romanelli[2], T. N. Todd[2], and JET Contributors†
EUROfusion Consortium, JET, Culham Science Centre, Abingdon, OX14 3DB, UK
[1]*Centre for Fusion, Space and Astrophysics,*
Department of Physics, University of Warwick, Coventry, UK
[2] *CCFE, Culham Science Centre, Abingdon, Oxfordshire OX14 3DB, UK*
[3]*Max-Planck-Institut für Plasmaphysik, Garching Germany*
[4]*Centre for the Analysis of Time Series,*
London School of Economics, London, UK and
[5]*Dept. of Engineering and Innovation,*
Open University, Milton Keynes, UK

(Dated: January 8, 2016)

Abstract

We perform direct time domain analysis of high time resolution signals from fast radial field coils and full flux azimuthal loops in JET. These toroidally integrating signals provide simultaneous high time resolution observation of global plasma dynamics and its coupling to the control system. We examine the time dynamics of these signals in plasmas where pellet injection is used to trigger ELMs in the presence of naturally occurring ELMs. ELM occurrence times are identified from BeII emission. Pellets whose size and speed are intended to provide maximum local perturbation for ELM triggering are launched at pre-programmed times, hence without correlation to the ocurrence times of intrinsic ELMs. Pellet rates were kept sufficiently low to prevent sustained changes of the underlying plasma conditions and natural ELM behaviour. We find a global signature of the build-up to natural ELMs in the temporal analytic phase of both the full flux loops and fast radial field coil signals. Before a natural ELM, the signal phases align to the same value on a $\sim 2-5ms$ timescale. We establish that this global build up to a natural ELM occurs whilst the amplitude of the full flux loop and fast radial field coil signals are at their background value: it precedes the response seen in these signals to the onset of ELMing. We perform the same analysis for ELMs that are the first to occur following pellet injection and find that in contrast to naturally occurring ELMs these signals do not clearly phase align before the ELM. This provides a direct test that can be used to distinguish when an ELM is triggered by a pellet as opposed to occurring naturally. It further supports the idea [1–4] of a global build up phase that precedes natural ELMs; pellets can trigger ELMs even when the signal phase is at a value when a natural ELM is unlikely to occur.

PACS numbers: 52.27.Gr, 52.35.Mw,52.55.Fa

*Electronic address: S.C.Chapman@warwick.ac.uk

†See the Appendix of F. Romanelli et al., Proceedings of the 25th IAEA Fusion Energy Conference 2014, Saint Petersburg, Russia

I. INTRODUCTION

Intense, short duration relaxation events known as edge localized modes (ELMs) [5–9] generally accompany enhanced confinement (H-mode) regimes in tokamak plasmas. Mitigation of large amplitude ELMs is essential for ITER because each ELM releases particles and energy which load the plasma facing components; scaled up to ITER[10], the largest such loads would be unacceptable. ELMs also play a role in removing impurities from the plasma, which should also be achieved in a controllable manner. The peeling-ballooning MHD instability at the plasma edge is believed to underlie the onset of an ELM burst [11–14] once local conditions for instability are reached. The sequence of events that leads to this remains an open question.

Empirically, longer waiting times between one ELM and the next broadly correlate with larger ELM amplitudes, so that proposals for mitigation include externally triggering many, smaller ELMs [15–17]. One method is to modify the conditions at the edge by injecting frozen deuterium pellets which quickly ionise [18–21]. Pellet ELM pacing relies on the triggering of an ELM by the strong local perturbation imposed by the ablated and deposited particles in the plasma edge. Whilst previously found to be very effective in a Carbon wall environment, recently it has been found that the triggering efficiency is greatly diminished when changing to an all-metal-wall. In particular, lag-times have been observed between pellet injection and subsequent ELM where pellets failed to trigger. Clearly, successful triggering conditions depend on some combination of critical plasma and pellet parameters. Investigations of the underlying physics of the pellet ELM triggering process require the capability to discriminate between successful and unsuccessful attempts to trigger an ELM with an injected pellet. The present paper focusses on a new, rigorous method for distinguishing whether an ELM appearing during or shortly after pellet ablations is triggered or is simply the chance occurrence of a natural ELM.

Quantitative characterization of the time domain dynamics of ELMing processes is relatively novel [22–27]. Recently [1–4] we found that for naturally occurring ELMs, the phase of the signals from a system scale diagnostic, the toroidally integrating full flux loops in the divertor region of JET, contains statistically significant information on the ELM occurrence times. The signal phases align to the same value on a $\sim 2-5ms$ timescale before each natural ELM occurs. This offers a potential direct diagnostic to distinguish pellet triggered

ELMs from those that occur naturally.

Here we focus on a JET plasma experiment in which ELMs are triggered by pellets in the presence of ELMs which occur naturally. We use a simultaneous high time resolution Be II signal to determine the ELM occurrence times. We perform direct time domain analysis of data from two sets of azimuthal coils for which there are high time resolution signals. The first set comprises full flux loops in the divertor region in JET, VLD2 and VLD3, their currents are proportional to the voltage induced by changes in poloidal magnetic flux. The second set is the current in the fast radial field coils (IFRFA), which are actively used for vertical stabilization of the plasma by the control system [27–29]. Taken together, these capture aspects of both the perturbation from the control system and the active global plasma response. We investigate the time dynamics of the signal temporal analytic phases, and directly test whether these signal phases contain information on the build-up to an ELM. We find that these signals do not clearly phase align before the pellet-triggered ELMs in these signals, whereas they do align for the natural ELMs within the same plasmas. This provides a direct test that can be used to distinguish when an ELM is triggered by a pellet, as opposed to occurring naturally. This result further supports the idea of a global build up phase to naturally occuring ELMs: pellets can trigger ELMs even when the signal phase is at a value when a natural ELM is unlikely to occur.

Since the fast radial magnetic field coils are part of the control system that actively maintains the plasma, our results also support the wider conjecture [1–4] that naturally occurring ELMs are precipitated by global plasma dynamics emerging from nonlinear feedback between plasma and control system.

II. DETAILS OF THE EXPERIMENT AND ANALYSED SIGNALS

We focus on one of a series of JET plasmas in which injected pellets were used to precipitate ELMs and where the occurrence frequency of naturally occurring ELMs far exceeded that of pellet injection. In JET plasma 86908 the plasma parameters are $I_P = 2.0MA$, $B_t = 2.1T$, $P_{NI} = 13MW$ and we analyse ELMs over the interval $9.0 - 20.7s$.

We analyse two sets of high (100 microsecond) time resolution toroidally integrating signals: (i) the current in the fast radial field coils (IFRFA), which are actively used for vertical stabilization by the control system; and (ii) voltages across passive full flux loops

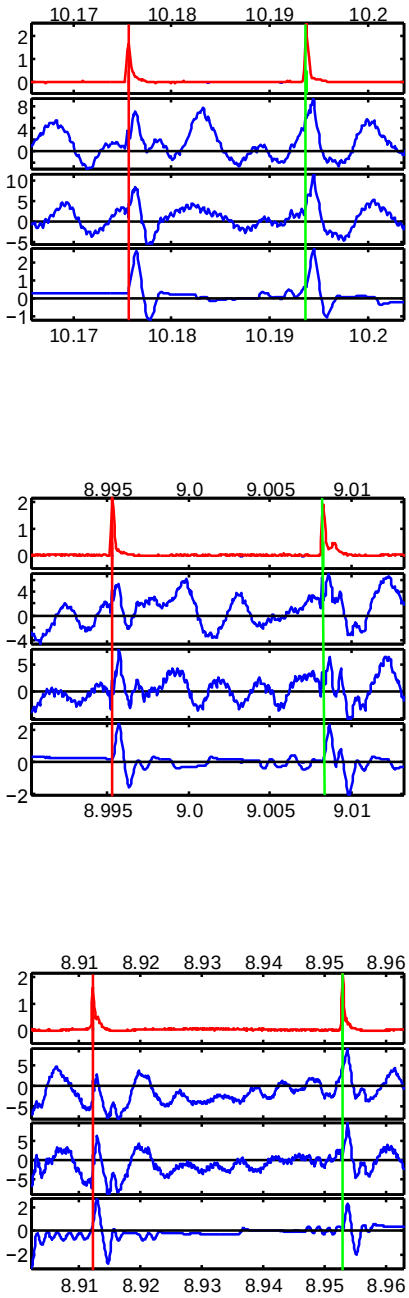

FIG. 1: Standardized traces of the raw timeseries for pairs of successive ELMs in JET plasma 86908. From top to bottom, time traces are plotted of: Be II intensity (red); full flux loops (blue) VLD2, VLD3; and fast radial field coil current IFRFA. To facilitate comparison we have standardized the signal amplitudes by dividing by a multiple of their respective means over the flat-top H-mode duration, and then subtracting a local mean. The occurrence times of sucessive ELMs are indicated by vertical red and green lines.

(VLD2 and VLD3). The VLD2 and VLD3 signals are the inductive voltage in the full flux loops which circle the JET tokamak toroidally at a location just below and outside the divertor coils[3]. They are directly proportional to the current in the full flux loops. These flux loops are passive, in that they input to the control system only. We present analysis of the VLD2 signal, and we repeated the analysis for the VLD3 signal and obtained the same results. The IFRFA signal is the current in the vertical control coils which circle the JET tokamak toroidally and are located at approximately 2/3 of the height of the vessel. The IFRFA flux loop is active, in that it both inputs and outputs to the active control system of the plasma.

We determine the ELM occurrence times t_k by identifying the peak of the Be II signal within each ELM using the method in [1]. We first calculate the 300 point running mean of the Be II signal excluding outliers, which are defined as lying outside 6 standard deviations. We then consider the signal to contain an ELM only where it exceeds this running mean by 2 standard deviations. To ensure that the largest peak is selected in regions where there are multiple local maxima, the ELM occurrence time is taken to be that of the maximum within a 50 data point window. This method does not distinguish ELMs that occur naturally from those that are triggered by pellet injection. We identify pellet triggered ELMs by searching for the first ELM identified by this algorithm that occurs following a pellet. The pellet times are identified by the strong D_a radiation emitted during pellet ablation, lasting for typically $1ms$ and recorded by wide angle diodes or fast framing cameras. For all the pellets in plasma 86908, using the Be II peak to define the ELM ocurrence time as above, an ELM is found to occur about $1ms$ after the pellet burn-out time. We will see that this is approximately the rise time of the VLD and IFRFA signals at the onset of the triggered ELM.

Sample timeseries of these (standardised amplitude) signals from plasma 86908 are shown in Figure 1, over time intervals extending over pairs of successive natural ELMs. The times t_k determined by this method are marked with vertical lines on the figure. There is a large bipolar response to each ELM in these signals which then decays away, however the signals continue to oscillate at a lower amplitude throughout the time interval between one ELM and the next. The passive full flux loop signal does not simply track the the active fast radial field coil signal. This difference reflects the plasma response; if the plasma is absent, as shown in Figure 2, the passive full flux loops do respond almost instantaneously to changes in the active fast radial field coil current. We will now directly obtain the instantaneous

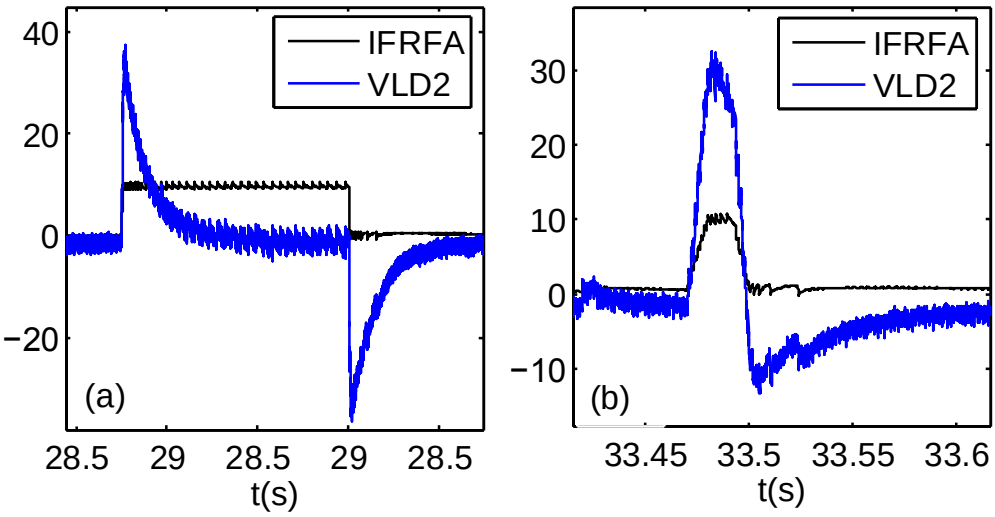

FIG. 2: Experiment 87095 on JET where the IFRFA is run through a test sequence with no plasma. The actively pulsed radial field coil (IFRFA, black) and full flux loop response (VLD2, blue) are plotted for two example test signals. The full flux loop response can be seen to track fast changes in the radial field coils, there is no observable lag. When the radial field coil current is held constant, the full flux loop has a decay time of $\sim 0.2s$.

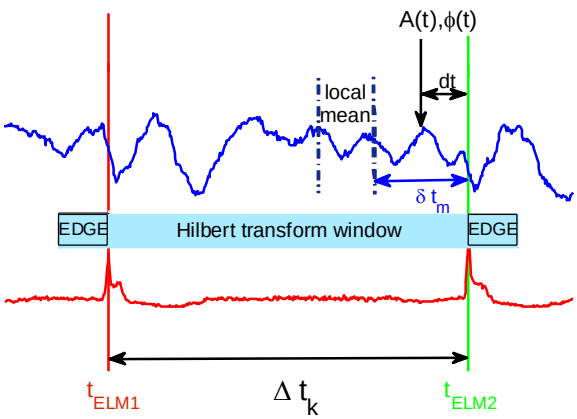

FIG. 3: Schematic (not to scale) of the procedure to determine the time dependent full flux loop difference in temporal analytic phase $\Delta\phi_k(\delta t)$ as a function of the time interval δt measured back from the time t_{ELM2} of the second ELM in an ELM pair. $\Delta\phi_k(\delta t)$ is calculated w.r.t the temporal analytic phase at the time of the first ELM in the entire sequence. The temporal analytic phase can only be determined at times that are within the Hilbert transform window edge δt_E.

temporal analytic amplitude and phase of these signals in order to test for information in these oscillations.

III. DETERMINATION OF INSTANTANEOUS TEMPORAL ANALYTIC AMPLITUDE AND PHASE

A time series $S(t)$ has a corresponding analytic signal defined by $S(t) + iH(t) = A\exp[i\phi(t)]$, where $H(t)$ is the Hilbert transform of $S(t)$, defined in [30, 31, 33] see also [32, 34]. This defines an instantaneous temporal analytic amplitude $A(t)$ and phase $\phi(t) = \omega(t)t$ where the instantaneous frequency is $\omega(t)$ for the real signal $S(t)$. We compute the analytic signal by Hilbert transform over each waiting time Δt_k between each pair of ELMs. The procedure is summarized in the schematic shown in Figure 3, which shows the domain over which the Hilbert transform is calculated relative to a pair of ELMs occurring at $t_{k-1} = t_{ELM1}$ and $t_k = t_{ELM2}$. We will obtain the temporal analytic phase for the full flux loop signals for a sequence of times δt preceding the second ELM of each pair, that is, at times $t_{ELM2} - \delta t$.

We first perform a 3 point spline smoothing on the VLD2, VLD3 and IFRFA time series to remove noise fluctuations on the sampling timescale and then subtract a local signal mean for the interval between each pair of ELMs as shown in Figure 1. A signal mean is determined locally in a $7.5ms$ sub-window which ends 2.5ms before t_{ELM2} The Hilbert transform has a single-sided Fourier transform which is approximated via fast Fourier transform over the finite time window of the data. We therefore use a time window that is larger than that of the time domain of interest to avoid edge effects. Here, the window extends beyond the time of the ELM. We have verified [3] that the phase alignment identified here in the global build up to an ELM can still be identified even if a window is chosen that does not extend to the time of the ELM. For a given pair of ELMs the time window is from $t_{ELM1} - 50ms$ to $t_{ELM2} + 50ms$ and we then only consider instantaneous amplitude and phase within the time interval t_{ELM1} to t_{ELM2}. Here, phase is defined relative to the phase ϕ_0 at which the first ELM in the entire sequence occurs so we will plot $\Delta\phi = \phi(t) - \phi_0$, where $t_0 = t_{ELM1}$.

The above method is only effective if the signals have good signal/noise, do not have too large a dynamic range in response to all the ELMs, and if the mean of the signal does not vary too rapidly. The high rate of change of instantaneous temporal analytic phase with

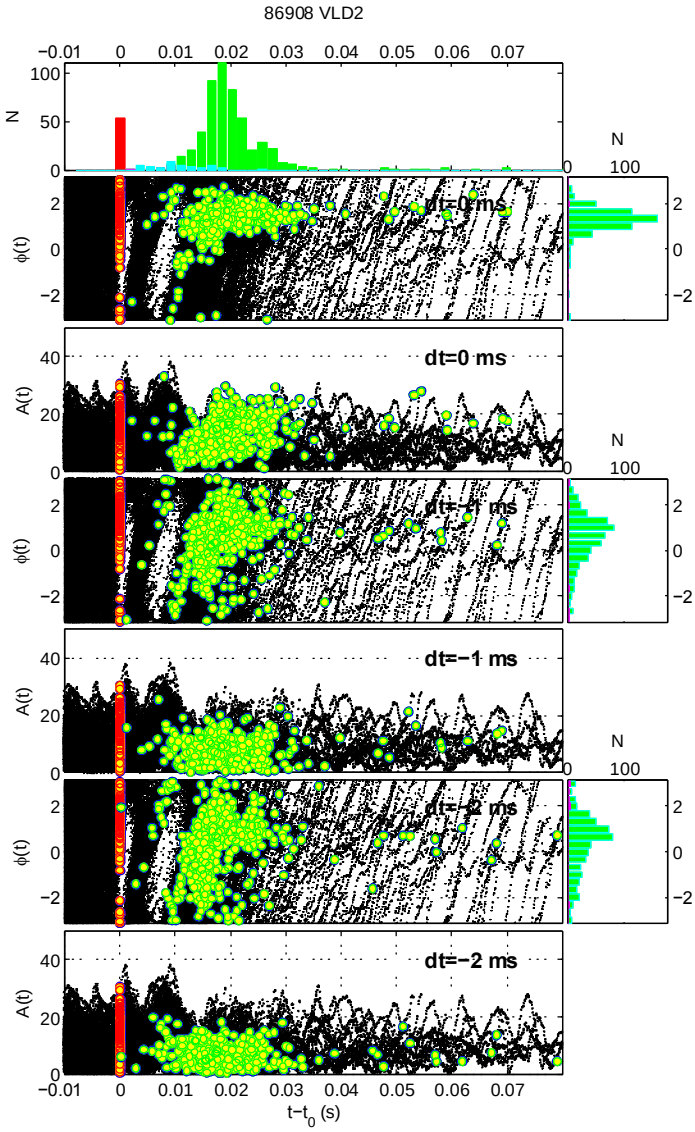

FIG. 4: ELM occurrence times and VLD2 and temporal analytic amplitude and phase shown for all naturally occurring ELMs in the flat-top of JET plasma 86908. The format of each set of panels is as follows: Main panel: VLD2 instantaneous temporal analytic phase, modulo 2π, plotted as a function of time following each ELM up to the occurrence time of the next ELM. The coordinates are relative time $\Delta t = t - t_0$ and difference in temporal analytic phase $\Delta\phi = \phi(t) - \phi_0$, where $t_0 = t_{ELM1}$ and ϕ_0 is the phase at which the first ELM in the entire sequence occurs. ELM occurrence times are marked on each VLD2 trace with yellow-filled red circles (first ELM) and yellow-filled green circles (second ELM). Right hand panel: histogram of VLD2 $\Delta\phi$ at the time of all the second ELMs (blue). Top panel: histogram of ELM occurrence times $\Delta t = t - t_0$ for the first ELM (red) and the second ELMs (green), overplotted (pink) for the prompt ELMs. The frequency N of first ELM times has been rescaled by 1/10.

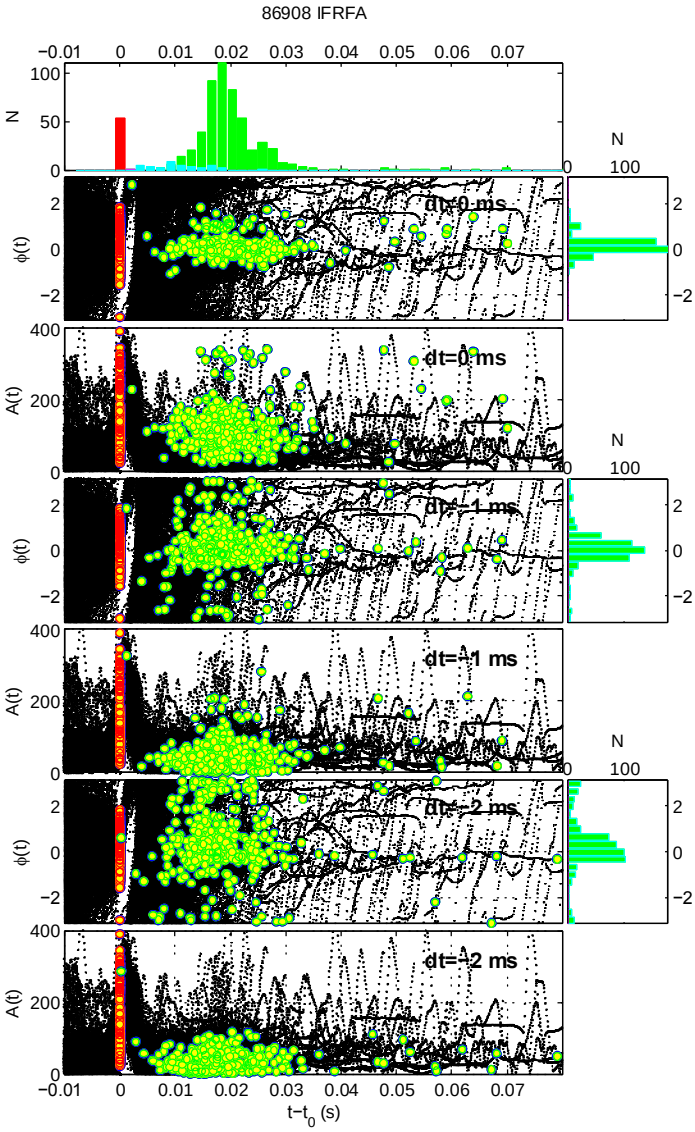

FIG. 5: ELM occurrence times and IFRFA temporal analytic amplitude and phase shown for all naturally occurring ELMs in the flat-top of JET plasma 86908. The format follows that of the previous figure.

time of the signals requires well defined ELM occurrence times in order to cleanly determine any phase relationship.

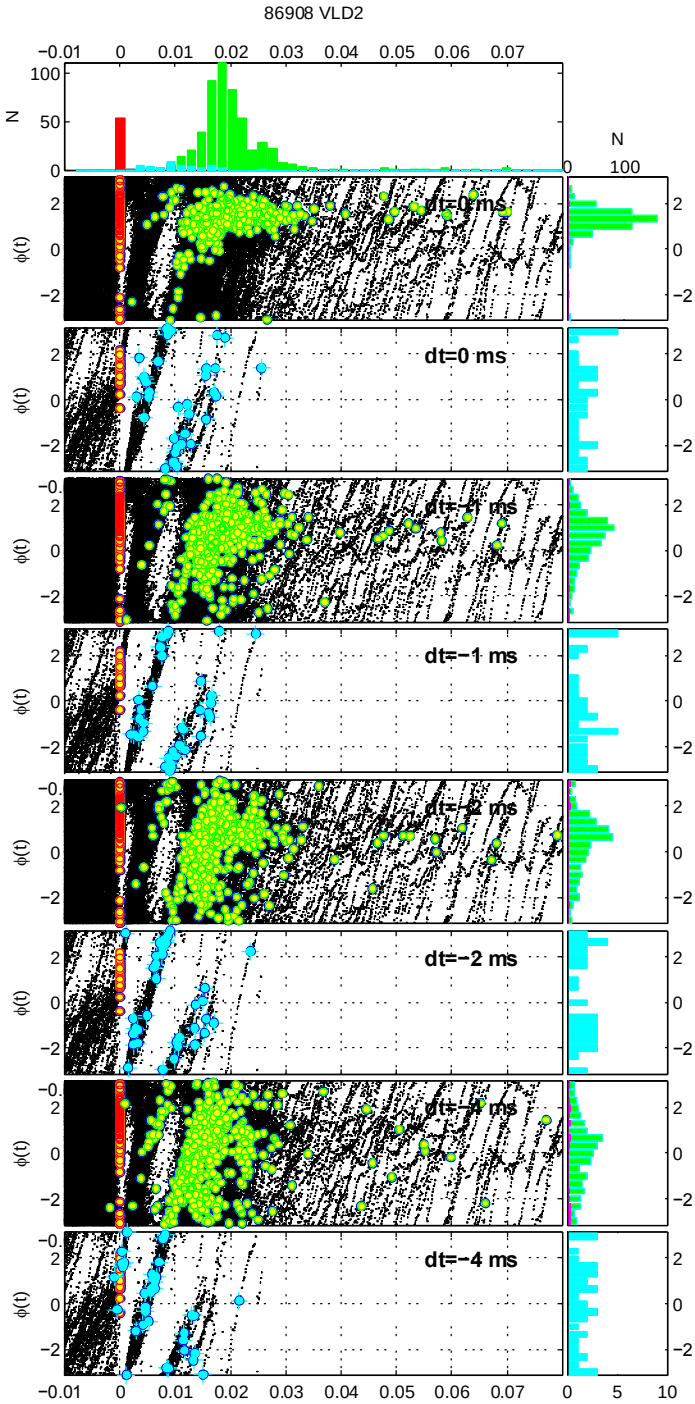

FIG. 6: ELM occurrence times and VLD2 temporal analytic phase plotted for the flat-top phase of JET plasma 86908. The format follows that of the previous figure, except that now all naturally occurring ELMs (green) and ELMs that occur following pellet injection (blue) are plotted separately. Note the different scales on the histograms of instantaneous phase plotted in the right hand panels.

IV. FULL FLUX LOOP INSTANTANEOUS TEMPORAL ANALYTIC PHASE AND BUILD-UP TO AN ELM

During plasma H-mode flat top there are a few hundred ELMs. Figures 4 and 5 plot how the instantaneous amplitude and phase of the VLD2 and IFRFA signals evolve from one ELM to the next for all the (570) ELMs in the H-mode flat top in plasma 86908. Alternating panels plot instantaneous amplitude and phase versus time. Here, all phases are measured from a single reference, the instantaneous phase of the signal at the time of the first ELM in the H-mode flat top. The phase at the occurrence time of each ELM is plotted at time zero and black traces plot the time evolving phases up to the occurrence time of the next ELM. The green circles plot the phase at time dt before the next ELM occurs, looking earlier in time (more negative dt moving down the plots). We then immediately see that the instantaneous phases are not random, they are phase-bunched. As we move back in time, the phases remain bunched and track back to progressively more negative values. The active fast radial field coil current that directly tracks the coupled control system and the plasma response thus contains within its instantaneous phase the signal of the build up to an ELM. The fact that the passive flux loop also detects such a signal, but does not simply track the signal of the active field coils, suggests that there is a nonlinearly coupled, synchronous dynamics between control system and plasma, and not simply a triggering of ELMs by the control system, as conjectured in [3].

We determine the ELM occurrence times from the Be II emission peak. The start of an ELM can also be seen in the response of the IFRFA and VLD signals. To distinguish the IFRFA and VLD sharp rise in response to an ELM from the build-up phase before an ELM, we examine the instantaneous amplitude at, and before, the ELM occurrence time. The rise time of the VLD2 and IFRFA response to the ELM is fast enough that it is possible that these signals are already responding to the ELM by the time the Be II reaches its peak. In Figures 4 and 5 we can see that at $dt = 0$, $t = t_{ELM2}$ (the Be II peak time) the instantaneous amplitude is for some ELMs comparable to the response to the previous ELM. At $dt = -1ms$ before the ELM, the signal amplitudes are for most ELMs closer to the unperturbed level and at $-2ms$ the amplitudes are generally at the unperturbed level. This confirms that the response to the ELM in the VLD2 and IFRFA occurs within 1-2ms just before the ELM time as determined by the peak in the Be II. At this time, the IFRFA

and VLD2 phases are bunched, suggesting that there is an indication of the build-up to an ELM in these global, toroidally integrating signals. We repeated this analysis for the VLD3 signal and obtained the same results.

We now distinguish naturally occurring ELMs from those that follow pellet injection. The corresponding figure for the VLD2 full flux loop is plotted in Figure 6. Here we have selected, and plotted as a separate population, the first ELM that occurs following the injection time of a pellet which is identified by the strong D_a radiation emitted during pellet ablation. Whilst the natural ELMs show the same phase alignment as above, the pellet triggered ELMs do not: they simply occur within $1ms$ of the pellet injection time, regardless of the value of the instantaneous phase of the VLD2 signal. This can be seen in the phase histograms on the right hand side of the figure and implies that the pellet triggered ELMs are empirically distinguishable, by this method, from the naturally occurring ELMs. In this plasma the number of ELMs following pellets (35) is much smaller than the total number of ELMs (570), on the Figure these histograms are on different scales. Let us now quantify the statistical significance of the alignment that we have identified.

V. CIRCULAR STATISTICS AND THE RAYLEIGH TEST

We use the Rayleigh test (see e.g. [35] and refs. therein) to quantify the extent to which the temporal analytic phase differences are aligned, and the statistical significance of any such alignment. Using the procedure described above, we determine the temporal analytic phase differences $\Delta\phi_k$ for the $k = 1...N$ ELM pairs in a given plasma. If each temporal phase is represented by a unit vector $\underline{r}_k = (x_k, y_k) = (cos\Delta\phi_k, sin\Delta\phi_k)$ then a measure of their alignment is given by the magnitude of the vector sum, normalized to N. This is most easily realized if we use unit magnitude complex variables to represent the $\underline{r}_k = e^{i\Delta\phi_k}$. Then the Rayleigh number is the magnitude of the sum:

$$R = \frac{1}{N} \mid \sum_{k=1}^{N} \underline{r}_k \mid = \frac{r}{N} \tag{1}$$

and the mean temporal analytic phase angle is $\bar{\phi}$. Clearly, if $R = 1$ the temporal phases are completely aligned.

An estimate of the p-value under the null hypothesis that the vectors are uniformly

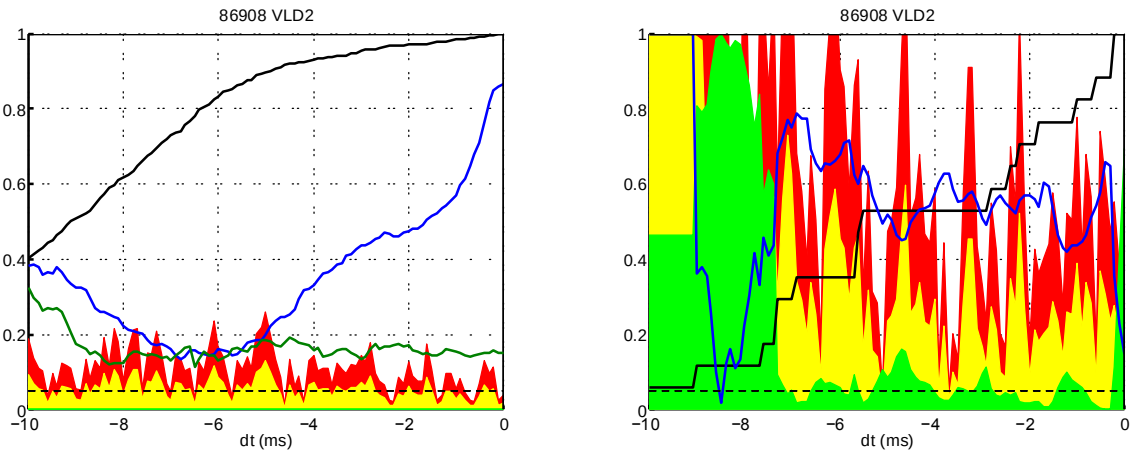

FIG. 7: Rayleigh statistics for VLD2 difference in temporal analytic phase $\Delta\phi$ just before an ELM in the flat-top of JET plasma 86908. Left panel is for all natural ELMs and right panel for all ELMs following injection of a pellet. The temporal analytic phase difference is calculated at time δt before the ELM and Rayleigh's R is plotted (y-axis) versus $-\delta t$ (x-axis). We plot R for the original timeseries (blue line) and two randomised surrogates: (i) the ELM waiting times have been shuffled (green line); (ii) the VLD2 timeseries has been shuffled (yellow shading is the R value and red shading $2 \times R$). The fraction of the total set of ELMs in the analysis is plotted with a black line. The corresponding p-value is indicated by the green filled shading, the $p = 0.05$ level is indicated by the horizontal dashed black line.

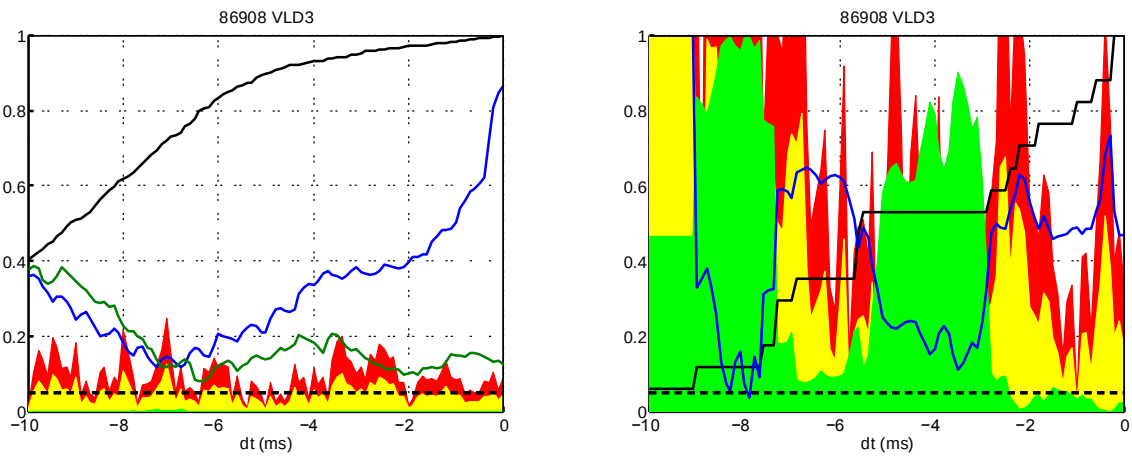

FIG. 8: Rayleigh statistics for VLD3 difference in temporal analytic phase $\Delta\phi$ just before an ELM in the flat-top of JET plasma 86908. Left panel is for all natural ELMs and right panel for all ELMs following injection of a pellet. The format is the same as the previous figure.

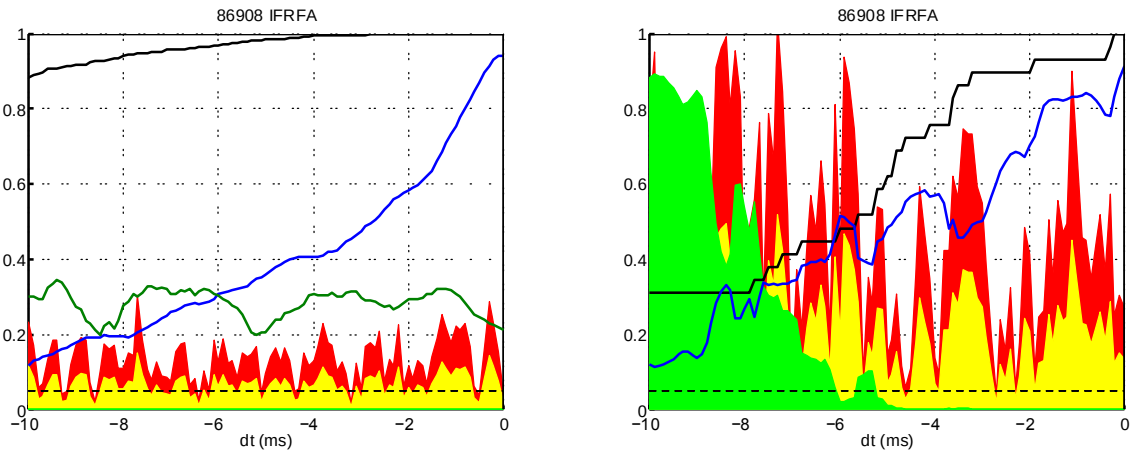

FIG. 9: Rayleigh statistics for IFRFA difference in temporal analytic phase $\Delta\phi$ just before an ELM in the flat-top of JET plasma 86908. Left panel is for all natural ELMs and right panel for all ELMs following injection of a pellet. The format is the same as the previous figure.

distributed around the circle is given by [35]:

$$p = exp\left[\sqrt{1 + 4N + 4N^2(1 - R^2)} - (1 + 2N)\right] \tag{2}$$

so that a small value of p indicates significant departure from uniformity, i.e. the null hypothesis can be rejected with 95% confidence for $p < 0.05$.

We now check that the above results are significant compared to a random process. First, we construct surrogate timeseries that randomise one property of the timeseries whilst retaining all others. The Rayleigh statistics of these surrogate timeseries are then plotted alongside those of the original timeseries. This analysis of the surrogate timeseries quantifies the likelihood of alternative hypotheses, where phase alignment has occurred by chance. Coincidental phase alignment could for arise for example in a finite data-set where both the sequence of ELM arrival times, and the full flux loop signals contain time structure that includes periodicity. This consideration is relevant to the present study, since ELM waiting times have a mean period and the full flux loop signals exhibit intervals of oscillatory behaviour.

Two surrogate timeseries are constructed here: (i) we randomly permute the time sequence of ELM waiting times and (ii) we randomly permute the time order of values in the VLD2,3 and IFRFA signals. For the first of these surrogates, for each ELM waiting time Δt_j we generate a surrogate ELM waiting time Δt_s by selecting at random from the

observed time sequence of ELM waiting times $\{\Delta t_1, \Delta t_2, ...\Delta t_j..\Delta t_N\}$, under the condition $\Delta t_s \leq \Delta t_j$. The surrogate set of ELM arrival times that this generates is $t_s = t_{j-1} + \Delta t_s$.

The Rayleigh statistics for the original and surrogate timeseries are plotted in Figures 7, 8 and 9 separately for ELMs that occur following pellet injection and all other, naturally occurring ELMs. A value of $R = 1$ indicates that all phases are exactly aligned, and our random surrogate shows that for the naturally occurring pellets $R \sim 0.1 - 0.3$ could arise by chance, it is the value obtained by shuffling the ELM occurrence times or the flux loop signals. It follows that that the rise in $R-$ value above 0.3 at $-4ms < dt < 0$ for the real data in Figures 7, 8 and 9 is statistically significant. Whereas the natural ELMs can be seen to progressively align as the ELM occurrence time $dt = 0$ is approached, the pellet triggered ELMs show no statistically significant alignment, they have highly variable values of R and these are comparable to what could occur by chance. For the VLD2 and 3 signals, $p \sim 0.05$ indicating that the null hypothesis of a uniform distribution of phases around the circle cannot be rejected. This is not the case for the IFRFA signal, which is far less sinusoidal in character and hence systematically dwells for longer periods at one or two phase values. However the R value for the IFRFA is comparable to that found for the surrogate timeseries where the signal is shuffled and hence does not indicate statistically significant alignment.

We have found that the details of where short-lived fluctuations in R and p-value occur are not robust, they vary with the dataset and with the detailed parameters of how the Hilbert transform is computed. However the overall trends are robust, in particular, alignment of the temporal analytic phases around a single value for $\delta t < 5ms$ for the naturally occurring ELMs.

VI. CONCLUSIONS

We analysed the signature of the global build-up to ELMs in JET plasmas where ELMs are triggered by pellet injection in the presence of ELMs that are naturally occurring; the natural ELM frequency exceeds that of the injected pellets. We have established a signature of the build-up to naturally ocurring ELMs in the temporal analytic phase of high time resolution signals: (i) full flux loops in the divertor region, and (ii) fast radial field coils that are part of the control system that actively stabilizes the plasma. These are toroidally integrating and hence capture global plasma dynamics. Before a natural ELM, the signal

phases align to the same value on a $\sim 2-5ms$ timescale. We establish that this global build up to a natural ELM occurs whilst the amplitude of the signals is at its background value; it precedes the response to the onset of ELMing. We perform the same analysis on ELMs which occur following pellet injection and find that these signals do not clearly phase align before the ELM. This result provides a direct test that can be used to distinguish when an ELM is triggered by a pellet as opposed to occurring naturally. It further supports the idea of a global build up phase to natural ELMs. In contrast, pellets can trigger ELMs even when the signal phase is at a value when a natural ELM is unlikely to occur.

This aspect of natural ELMing is consistent with a nonlinear feedback between control system and plasma to generate the global plasma dynamics that then precipitates an ELM. Coherent global dynamics emerges from the background fluctuations in the active control system field coil current and passive full flux loops. If there were coupling between the control system and each of several growing perturbations in the plasma, these perturbations could become synchronized [32–34], through their individual interactions with the control system without the need of coupling between them.

Acknowledgments

We acknowledge the EPSRC for financial support. This work has been carried out within the framework of the EUROfusion Consortium and has received funding from the Euratom research and training programme 2014-2018 under grant agreement No 633053. The views and opinions expressed herein do not necessarily reflect those of the European Commission.

[1] S. C. Chapman, R. O. Dendy, T. N. Todd, N. W. Watkins, A. J. Webster, F. A. Calderon et al., Phys. Plasmas 21 062302 (2014)

[2] S. C. Chapman, R. O. Dendy, A. J. Webster, N. W. Watkins, T. N. Todd, J. Morris and JET EFDA Contributors, 41st EPS Conference on Plasma Physics, June 2014, EPS Vol. 38F ISBN 2-914771-90-8, European Physical Society (2014) http://ocs.ciemat.es/EPS2014PAP/pdf/P1.010.pdf

[3] S. C. Chapman, R. O. Dendy, T. N. Todd, N. W. Watkins, F. A. Calderon, J. Morris, and JET Contributors, The global build-up to intrinsic ELM bursts seen in divertor full flux loops

in JET, Phys. Plasmas 22, 072506 (2015)

[4] S C Chapman, R O Dendy, N W Watkins, T N Todd, F A Calderon and JET Contributors, ELM occurrence times in relation to the phase evolution of global measurements in JET, Proceedings, 42nd EPS Conference on Plasma Physics, June 2015, EPS Vol. 39E ISBN 2-914771-98-3, European Physical Society (2015)

[5] M. Keilhacker, Plasma Phys. Control. Fusion 26, 49 (1984).

[6] V. Erckmann, F. Wagner, J. Baldzuhn, R. Brakel, R. Burhenn, U. Gasparino, P. Grigull, H. J. Hartfuss, J. V. Hofmann, R. Jaenicke et al. Phys. Rev. Lett. 70, 2086 (1993).

[7] H. Zohm, Plasma Phys. Control. Fusion 38, 105 (1996).

[8] A. Loarte , G. Saibene, R. Sartori, D. Campbell, M. Becoulet, L. Horton, T. Eich, A. Herrmann, G. Matthews, N. Asakura, A. Chankin, A. Leonard, G. Porter, G. Federici, G. Janeschitz, M. Shimada, M. Sugihara et al, Plasma Phys. Control. Fusion 45, 1549 (2003).

[9] K. Kamiya, N. Asakura, J. Boedo, T. Eich, G. Federici, M. Fenstermacher, K. Finken, A. Herrmann, J. Terry, A. Kirk, B. Koch, A. Loarte, R. Maingi, R. Maqueda, E. Nardon, N. Oyama. R. Sartori, Plasma Phys. Control. Fusion 49, S43 (2007).

[10] R.J. Hawryluk, D.J. Campbell, G. Janeschitz, P.R. Thomas, R. Albanese, R. Ambrosino4, C. Bachmann, L. Baylor, M. Becoulet, I. Benfatto, J. Bialek et al., Nucl. Fusion, 49, 065012, (2009)

[11] J. W. Connor, Plasma Phys. Control Fusion 40 191 (1998)

[12] Snyder P.B., Wilson H.R., Ferron J.R., Lao L.L., Leonard A.W., Osborne T.H., Turnbull A.D., Mossessian D., Murakami M. and Xu X.Q., Phys. Plasmas 9 2037 (2002)

[13] Saarelma, S., A Alfier, M N A Beurskens, R Coelho, H R Koslowski, Y Liang, I Nunes and JET EFDA contributors, MHD analysis of small ELM regimes in JET, PPCF 51, 035001 (2009)

[14] G. S. Yun, W. Lee, M. J. Choi, J. Lee, H. K. Park, B. Tobias, C. W. Domier, N. C. Luhmann, Jr., A. J. H. Donn, J. H. Lee, and (KSTAR Team), Phys. Rev. Lett., 107, 045004 (2011)

[15] E. de la Luna et al, Proceedings of the 36th EPS Conference on Plasma Physics, Sofia, Bulgaria. 29th June 2009 - 3rd July 2009

[16] P. T. Lang et al, Plasma Phys. Cont. Fusion, 46, L31L39, (2004)

[17] F. Sartori et al, 35th EPS Conference on Plasma Phys. Hersonissos, 9 - 13 June 2008 ECA Vol.32D, P-5.045 (2008) (2008)

[18] P. T. Lang, K. Bchl, M. Kaufmann, R. S. Lang, V. Mertens, et al., Phys. Rev. Lett. 79, 1487 (1997)

[19] P. T. Lang, B. Alper, L. R. Baylor, M. Beurskens, J. G. Cordey,R. Dux, et al. Plasma Phys. Cont. Fusion 44, 1919 (2002)

[20] P. T. Lang, J. Neuhauser,L. D. Horton, et al., Nuc. Fusion, 43, 10, 1110 (2003)

[21] P.T. Lang, G.D. Conway, T. Eich, L. Fattorini, O. Gruber, et al., Nuc. Fusion, 44, 665 (2004)

[22] A. W. Degeling, Y. R. Martin, P. E. Bak, J. B. Lister, and X. Llobet, Plasma Phys. Cont. Fusion 43, 1671 (2001).

[23] J. Greenhough, S. C. Chapman, R. O. Dendy, and D. J. Ward, Plasma Phys. Cont. Fusion 45, 747 (2003).

[24] F. A. Calderon, R. O. Dendy, S. C. Chapman, A. J. Webster, B. Alper, R. M. Nicol and JET EDFA Contributors, Phys. Plasmas, 20, 042306 (2013)

[25] A. J. Webster and R. O. Dendy, Phys. Rev. Lett. 110, 155004 (2013)

[26] A. J. Webster, R. O. Dendy, F. Calderon, S. C. Chapman, E. Delabie, D. Dodt, R. Felton, T. Todd, V. Riccardo, B. Alper, S. Brezinsek, et al, Plasma Phys. Control. Fusion, 56, 075017 (2014)

[27] A Murari, F Pisano, J Vega, B Cannas, A Fanni, S Gonzalez, M Gelfusa, M Grosso and JET EFDA Contributors, Plasma Phys. Control. Fusion 56, 114007 (2014)

[28] A. Murari, E. Peluso, P. Gaudio, M. Gelfusa, F. Maviglia, N. Hawkes and JET-EFDA Contributors, Plasma Phys. Control. Fusion 54, 105005 (2012)

[29] A. Neto et al, 2011 50th IEEE Conference on Decision and Control and European Control Conference (CDC-ECC) Orlando, FL, USA, December 12-15, (2011)

[30] D. Gabor, Proc. IEE, vol. 93 (III), pp. 429457, (1946)

[31] R. N. Bracewell, *The Fourier transform and its applications, 2nd Ed.* (McGraw Hill, 1986)

[32] M. G. Rosenblum, A. S. Pikovsky, J. Kurths, Phys. Rev. Lett, 76, 1804, (1996)

[33] A. Pikovsky, M. G. Rosenblum, J. Kurths, *Synchronization: a universal concept in nonlinear sciences*, C.U.P., (2003)

[34] J. T. C. Schwabedal, A. S. Pikovsky, Phys. Rev. Lett., 110, 24102 (2013)

[35] N. I. Fisher, *Statistical Analysis of Circular Data. Revised edition.* Cambridge University Press.(1995)